Diamond & Related Materials 132 (2023) 109650

Contents lists available at ScienceDirect

Diamond & Related Materials

journal homepage: www.elsevier.com/locate/diamond

Tribological behavior of silicon and oxygen *co*-doped hydrogenated amorphous carbon coatings on polyether ether ketone

Xianchun Jiang [a,b], Peng Guo [b], Li Cui [b], Yadong Zhang [b], Rende Chen [b], Yumin Ye [a], Aiying Wang [b,c], Peiling Ke [b,c,*]

[a] Faculty of Materials Science and Chemical Engineering, Ningbo University, Zhejiang, Ningbo 315211, China
[b] Key Laboratory of Marine Materials and Related Technologies, Zhejiang Key Laboratory of Marine Materials and Protective Technologies, Ningbo Institute of Materials Technology and Engineering, Chinese Academy of Sciences, Ningbo 315201, China
[c] Center of Materials Science and Optoelectronics Engineering, University of Chinese Academy of Sciences, Beijing 100049, China

ARTICLE INFO

Keywords:
Polyether ether ketone
Amorphous hydrogenated carbon coating
Si/O doping
Tribological properties
Mechanical properties

ABSTRACT

Polyether ether ketone (PEEK) is widely used for polymer-metal sliding pairs due to its excellent characteristics such as self-lubrication, and chemical stability. However, PEEK is prone to be worn easily when it comes to friction with metal, which is the most critical limitation for the development of PEEK/metal tribo-pairs. In this study, the tribological properties of silicon and oxygen co-doped amorphous hydrogenated carbon (a- C:H:Si:O) coating on PEEK substrates were focused, where the a-C:H was used for comparison simultaneously. Results revealed that both a-C:H and a-C:H:Si:O coated PEEK displayed a high hardness over 6 GPa and enhanced the tribological resistance. Noted that even the PEEK coated with a-C:H coating behaved the lowest wear rate of 1.82 $\times$ 10^{-7} mm^3/Nm, co-doping Si and O improved the adhesion strength between coating and PEEK substrate together with the lubricity. In particular, the a-C:H:Si:O coatings with the concentration of 3.96– 7.49 at. % for Si and 3.07– 6.07 at. % for O showed excellent stability with a wear rate of (2.9 $\pm$ 0.4) $\times$ 10^{-7} mm^3/Nm, due to the formed compacted tribo-film over the counterpart. The results bring forward a promising strategy to enhance the wear resistance of PEEK/metal sliding components for harsh tribological applications.

1. Introduction

Polyether ether ketone (PEEK) is a high-performance thermoplastic polymer material, which has outstanding self-lubrication characteristics, high toughness-stiffness, fatigue resistance, and chemical stability [1–4]. Therefore, it has been widely used in polymer-metal sliding pairs [5,6]. Nevertheless, for pristine PEEK, its mechanical strength and thermal stability are lower than that of the metallic counterpart. The resulting poor wear resistance, high coefficient of friction, and local melting of the PEEK can greatly restrict its booming in engineering applications. Therefore, some modification methods should be considered for improving the tribological performance of the PEEK-metal tribo-pair [7].

Generally, both adding appropriate fillers and surface modification treatments are employed to improve the tribological properties of PEEK. For example, Yan et al. [8] found that the addition of graphene oxide (GO) can reduce the friction coefficient and wear rate of PEEK, due to the improvement of hardness and tensile strength. Zhu et al. [9] also confirmed that adding the combination of carbon fiber, graphite, and polytetrafluoroethylene (PTFE) into PEEK would improve its self-lubricating performance, but reduce its wear resistance. By introducing nanometer silicon carbide, Wang et al. [10] believed that the improvement of the tribological properties of PEEK after modification was related to the formation of transfer film. Besides, the tribological performance of PEEK can be greatly improved by surface treatment methods without changing its excellent mechanical properties. Chen et al. [4] found that high laser power density treatment of PEEK can carbonize its surface and produce a solid lubrication effect, thus reducing its friction and wear. Using a picosecond laser to make dimples on PEEK, Wang and co-workers [11] concluded that when the dimple diameter was 50 mm, wear debris could be squeezed into texture dimples, avoiding the generation of large wear debris to reduce wear.

In particular, amorphous carbon has attracted much interest in this area, in consideration of its excellent hardness, high wear resistance, and

* Corresponding author at: Key Laboratory of Marine Materials and Related Technologies, Zhejiang Key Laboratory of Marine Materials and Protective Technologies, Ningbo Institute of Materials Technology and Engineering, Chinese Academy of Sciences, Ningbo 315201, China.
E-mail address: kepl@nimte.ac.cn (P. Ke).

https://doi.org/10.1016/j.diamond.2022.109650
Received 14 October 2022; Received in revised form 29 November 2022; Accepted 20 December 2022
Available online 26 December 2022

low friction coefficients, especially when sliding with metallic friction pair [12–15]. For example, Kaczorowski et al. [16] deposited amorphous hydrogenated carbon (a-C:H) on PEEK by radio frequency plasma-enhanced chemical vapor deposition (PECVD) method, and the wear rate of PEEK was reduced by 35 times. Su et al. [17] also prepared a-C:H on the surface of PEEK, and improved the adhesion strength of the coating on the substrate by etching PEEK. However, some researchers proposed that the high internal stress of a-C:H and its poor interface match with the polymer weakened the modification effect of a-C:H on PEEK [18–21]. It remains a challenge to avoid early fracture and delamination for a-C:H coated PEEK. Many researchers have attempted to solve this dilemma by reducing stress and designing an appropriate interface, such as introducing doping elements and transition layers [17,22–25]. Especially, the Si incorporation in diamond-like carbon (DLC) coating contributes to lower stress. The results show that the modified fluoro rubber with Si-DLC has a lower friction coefficient and wear rate [26]. Oxygen-doped modification treatment has also been proven to improve the adhesion strength of polymer composites [27]. Moreover, the silicon and oxygen co-doped a-C:H (a-C:H:Si:O) also showed reduced stress and improved thermal stability [25]. Considering these features, co-doping silicon and oxygen in a-C:H is considered one of the promising strategies for improving the tribological performance of PEEK. However, few studies have focused on the tribological properties of a-C:H:Si:O coated PEEK, their design criteria and the influence of silicon and oxygen concentration have yet to be disclosed.

In this work, a-C:H and a-C:H:Si:O coatings with different Si/O concentrations were deposited on PEEK, with the PECVD technique (Fig. 1). The mechanical and tribological properties of the a-C:H:Si:O coated PEEK were studied systematically, and the related failure mechanism was also discussed, which may provide an effective strategy for improving the performance of PEEK/metal tribo-pairs in engineering applications.

2. Material and method

2.1. Coating deposition

The coatings were prepared on both P-type Si (100) wafers and PEEK substrates (22 mm × 22 mm × 6 mm) by the PECVD technique, using acetylene (C_2H_2) and hexamethyl disiloxane (HMDSO) as the precursor gases. Before being loaded onto the substrates holder in the deposition chamber, the substrates were ultrasonically cleaned with ethanol for 10 min. When the chamber vacuum reached 4×10^{-3} Pa, all substrates were in-situ cleaned using an Ar plasma etch for 10 min to remove the adhered contamination, with a negative pulse voltage (Advanced Energy, plus +5 K) of 500 V. During deposition, the negative pulse voltage was kept at 450 V, and then the a-C:H/a-C:H:Si:O coatings were deposited, with 150 W pulse power and a duty cycle of 61.5 %. The substrates were not heated during deposition. The coatings were named S1 ~ S6, according to the gas flow ratio of HMDSO to C_2H_2. The gas flow rates were controlled by respective mass flow controllers and mixed before entering the deposition chamber with different mixture ratios. Before depositing the coating, we calculated the deposition rate of the coating under different gas ratios through exploratory experiments. A surface profilometer (Alpha-step IQ, USA) was used to measure the thickness of coatings. The results show that the deposition rate of the coating increased with the incorporation of HMDSO. With 100 sccm C_2H_2, a-C:H (S1) coating had the lowest deposition rate of 14.6 nm/min. As the gas flow ratio of HMDSO to C_2H_2 increased from 1/10 to 1/2, the corresponding deposition rate of the coatings also increased from 16.1 nm/min to 21.4 nm/min. By adjusting the deposition time, the thicknesses of all a-C:H/a-C:H:Si:O coatings were controlled to be approximately 1.5 μm. Detailed process parameters are shown in Table 1.

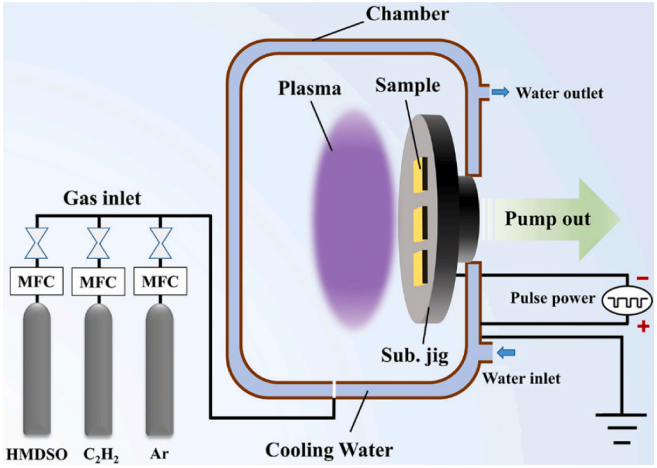

Fig. 1. Schematic diagram of PECVD system for a-C:H:Si:O deposition.

2.2. Microstructural and mechanical characterization

The composition content and chemical bonding state of the coatings were measured by X-ray photoelectron spectroscopy (XPS, Axis UltraDLD, Japan) with Al (mono) Kα radiation. To exclude the influence of surface impurities, Ar plasma was used to etch the target area for 30 s before the test. The Raman spectra (In Via-reflex, Renishaw) of the coatings were obtained with a 532 nm exciting wavelength laser. The coating on the silicon wafer was selected for the above characterization.

The hardness (H) and elastic modulus (E) of the coatings on PEEK substrates were measured by the MTS nanoindentation system (G200), which was equipped with a 20 nm radius Berkovich diamond tip using continuous stiffness mode. For each sample, the indentation depth was 200 nm. Accoring to *The model of Oliver and Pharr* [28], the H and E of the coatings were calculated from indentation load-displacement data. We randomly test several different positions on each sample surface and calculate the average value to ensure the uniformity and correctness of the data.

The scratch tester (CSM Revetest) equipped with a tapered diamond indenter (Φ = 0.2 mm) was used to test the adhesion strength between the coating and PEEK substrate. The indenter moved at a speed of 1 mm/min for a distance of 5 mm. At the same time, the applied load linearly increased from 1 to 30 N, with a loading speed of 5.8 N/min.

2.3. Friction and wear tests

A ball-on-plate tribometer (UMT-3) was used to evaluate the tribological performance of the coated PEEK in ambient air. A 304 stainless steel ball with a diameter of 6 mm was selected as the counterpart. The amplitude was 5 mm, and the sliding frequency was 5 Hz, corresponding to a velocity of 2.5 cm · s^{-1}. The load of 3 N was applied through a stationary loading system. The total reciprocating test duration was 1800 s. After the test, the normalized wear rate (W, $mm^3/N \cdot m$) was obtained according to the following equation [29]:

$$W = \frac{V}{FL} \tag{1}$$

where V is the wear volume loss (mm^3), F is the applied load (N), and L is the total sliding distance (m). The volume loss (V) of the coatings and the mating balls was calculated using the following equations [30]:

$$V_{coating} = l \times S \tag{2}$$

$$V_{ball} = (\pi h/6) \times \left(3d^2/4 + h^2\right) \tag{3}$$

where l is the amplitude (mm), S is the cross-sectional area of the wear track (mm^2), and d is the diameter of the wear scar (mm). The $h = r - (r^2 - d^2/4)^{1/2}$, where r is the radius of the mating balls (mm).

Table 1
Detailed process parameters of prepared a-C:H/a-C:H:Si:O coatings.

Samples	Negative pulse Voltage (V)	Current (A)	Chamber Pressure (Pa)	HMDSO (sccm)	C_2H_2 (sccm)	Deposition Rate (nm/min)	Deposition Time (min)
S1	450	0.3	2	–	100	14.6	102
S2				10	100	16.1	90.5
S3				10	80	16.6	88.7
S4				10	60	18.2	84
S5				10	40	19.5	77.5
S6				10	20	21.4	68

The two-dimensional (2D) wear track depth profiles of the coatings were measured by white light interferometer microscope (UP-Lambda). The surface topography and chemical composition of the coatings as well as the counterparts after friction tests were investigated by a field emission FEI Quanta FEG 250 scanning electron microscope (SEM), and the areal distributions of C, O, Si, and Fe elements on the counterparts were ascertained by energy dispersive X-ray spectroscopy (EDS). The transfer materials on the mating balls were analyzed by Raman spectroscopy with a laser wavelength of 532 nm.

3. Results

3.1. Composition and microstructure characteristics

The elements composition and bonding state of the deposited coatings were investigated by XPS. Fig. 2(a) illustrates the relative contents (at.%) of C, Si, and O elements. For a-C:H, only C, and a few O can be detected; as the HMDSO/C_2H_2 ratio increased from 1/10 to 1/2, the concentration of C decreased monotonously from 93.0 at.% to 79.8 at.%, while, the Si and O concentration increased from 4.0 at.% to 10.0 at.%, and from 3.1 at.% to 10.9 at.%, respectively. Fig. 2(b) shows the C 1s spectra of the a-C:H and a-C:H:Si:O coatings. In each C 1s spectrum, two peaks situated at 285.2 ± 0.1 eV and 286.5 ± 0.1 eV were ascribed to the sp^3-C and C—O bonds, respectively. The peak with a binding energy of 284.7 ± 0.1 eV corresponded to sp^2-C or C-Si-O bonds as reported in organosiloxanes [31]. The Si 2p spectrum of all a-C:H:Si:O coatings and its fitting results were shown in Fig. 2(c), it can be deconvoluted into three peaks centered at 100.9 ± 0.2 eV, 101.5 ± 0.2 eV, and 102.4 ± 0.2 eV, which were related to Si—C, Si $(—O)_1$ and Si$(—O)_2$, respectively [32]. The contents of sp^2-C/C-Si-O, sp^3-C, and C—O phases were shown in Table 2. The a-C:H had the maximum sp^3-C fraction of 38.6 at.%. With increasing Si and O concentration, the sp^3-C fraction in a-C:H:Si:O kept stable around 22.9 at.%, while, the C—O fraction of S6 significantly decreased at the highest HMDSO/C_2H_2 ratio.

Fig. 3 shows Raman spectra of a-C:H and a-C:H:Si:O coatings. In Fig. 3(a), for all samples, the G peak appeared at around 1530 cm^{-1}, which stemmed from the E_{2g} C—C stretching vibration, and the D peak appeared at around 1330 cm^{-1} due to the disordering of ordered graphite. The G and D peaks were fitted using two Gaussian modes. The

Table 2
The contents of sp^2-C/C-Si-O, sp^3-C, and C—O phases.

Samples	sp^2-C/C-Si-O (%)	sp^3-C (%)	C-O (%)
S1	53.8	38.6	7.6
S2	69.7	20.7	9.6
S3	69.3	22.9	7.8
S4	68.5	22.4	9.1
S5	65.5	26.8	7.7
S6	68.5	27.3	4.2

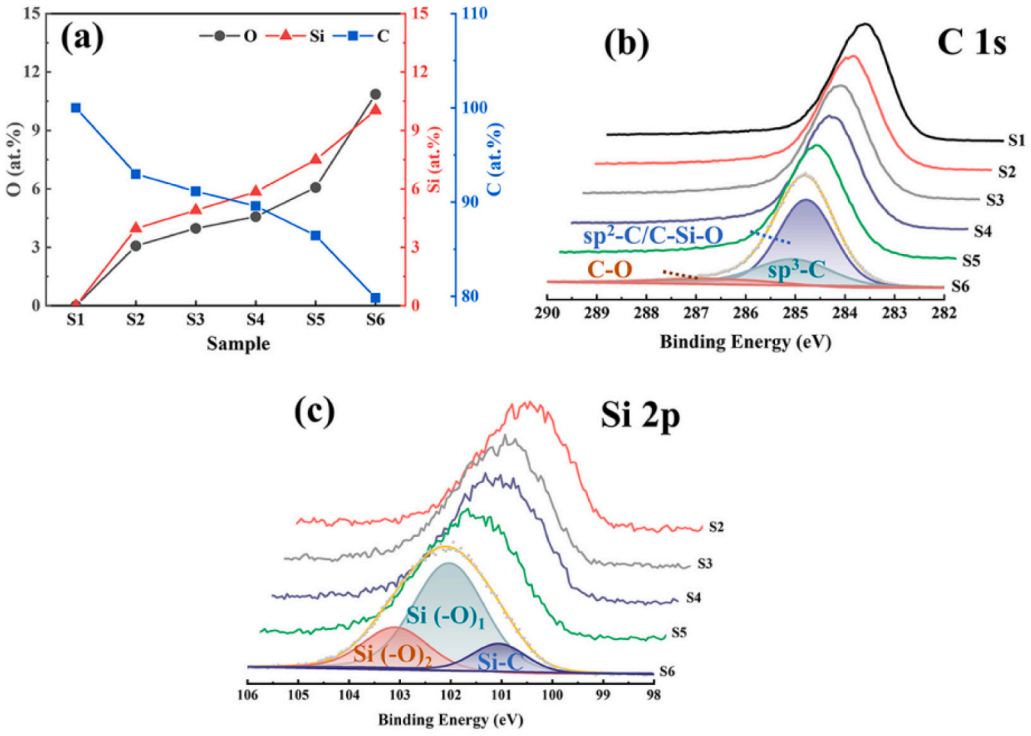

Fig. 2. The XPS spectra for (a) Chemical composition (calculated from XPS data) of coatings. (b) C 1 s and the C spectrum fitting result of coatings. (c) Si 2p and the Si spectrum fitting result of coatings.

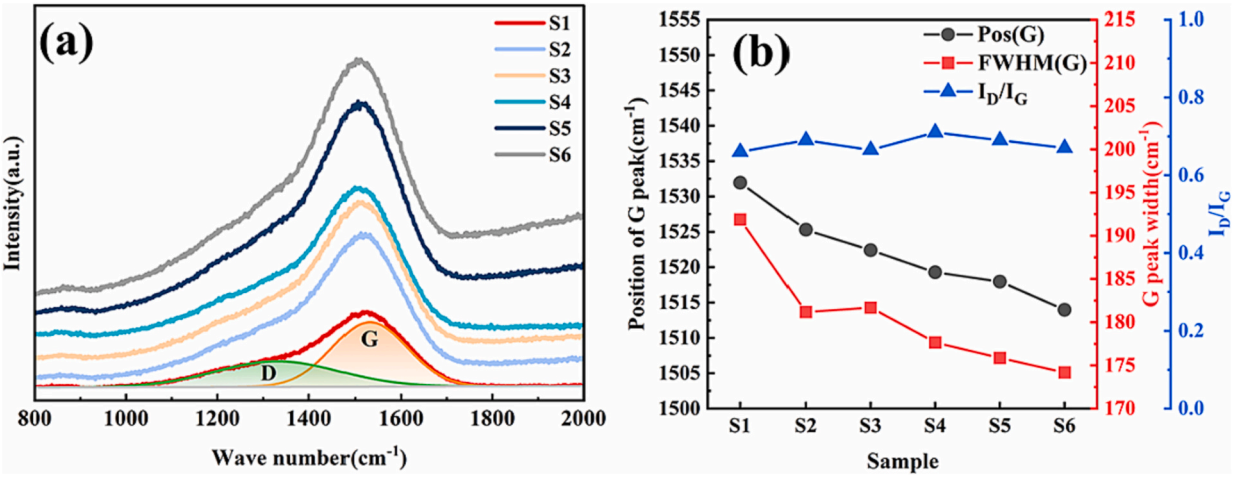

Fig. 3. (a) Raman spectra and (b) fitting results of a-C:H/a-C:H:Si:O coatings.

position of the G-peak, the full width at half maximum of G-peak (FWHM (G)), and the area ratio of D peak to G peak (I_D/I_G) were present in Fig. 3(b). With increasing silicon and oxygen contents, the position of the G-peak decreased from 1532 cm^{-1} to 1514 cm^{-1}, which suggested the decline of the sp^2 content, since the Si atoms can replace the C atoms and weaken the strength of C═C bonds [33]. FWHM (G) also decreased evidently from 191.9 cm^{-1} to 174.2 cm^{-1}, suggesting a more orderly structure. Meanwhile, a-C:H and a-C:H:Si:O coatings had approximate I_D/I_G values around 0.68, indicating the similar size of sp^2 clusters.

3.2. Mechanical properties

Hardness (H) and elastic modulus (E) are considered to be important parameters affecting the wear resistance of materials [34]. As shown in Fig. 4(a), the a-C:H coating exhibited a much higher H and E value than that of a-C:H:Si:O coatings, which were 10.4 and 49.5 GPa. With the increase of Si and O content, both the H and E of the coating decreased. The H values of the a-C:H:Si:O (S2 ~ S6) coatings were 8.3, 8.0, 7.8, 6.3, and 6.2 GPa, respectively, and the corresponding E values were 36.9, 36.7, 35.1, 32.2 and 29.8 GPa. The load-displacement curves of all samples can be found in supporting information Fig. S1. In Fig. 4(b), the H/E and H^3/E^2 were calculated, which can be used to evaluate the long-term durability, strain resistance, and plastic deformation resistance of coatings [35,36]. The high H/E ratio means that the coating has good elastic deformation resistance, and a high H^3/E^2 value indicates a higher plastic deformation resistance and better wear resistance [37,38]. The H/E ratio of the coatings did not change regularly. Samples 2 and 4 deposited with 1/10 and 1/6 gas flow ratios had the maximum H/E value of 0.22. However, the H^3/E^2 value exhibited obvious dependency on the silicon and oxygen content. The a-C:H coating sample showed the maximum H^3/E^2 value of 0.48. With increasing the doping content, the a-C:H:Si:O coatings showed a decreasing trend of H^3/E^2 value.

Fig. 5(a) shows the scratch morphologies of the coatings. Here, the critical load corresponding to the first visible crack on the coating surface in the scratch test is represented by L_{C1} [39,40]. The L_{C1} of the a-C:H and a-C:H:Si:O coated PEEK were about 3.0 N, 3.3 N, 4.8 N, 8.1 N, 7.8 N, and 6.0 N, respectively. When the crack was initiated, the corresponding acoustic emission signal was also generated (Fig. 5(b)). The incorporation of Si and O can greatly improve the adhesion strength between the a-C:H:Si:O coating and the PEEK substrate, which may be due to the increase of surface energy by its polar components [41,42]. While, once the oxygen content exceeded 10 at.%, the adhesion strength decreased slightly, which can be explained by the reduction of C—O bond formation [18], as confirmed by the above-mentioned XPS results.

3.3. Tribological test

Fig. 6(a) presents the friction coefficient (COF) curves for all coatings. Fig. 6(b) shows the average COF after the running-in stage and the wear rate of a-C:H and a-C:H:Si:O coatings. Supporting information

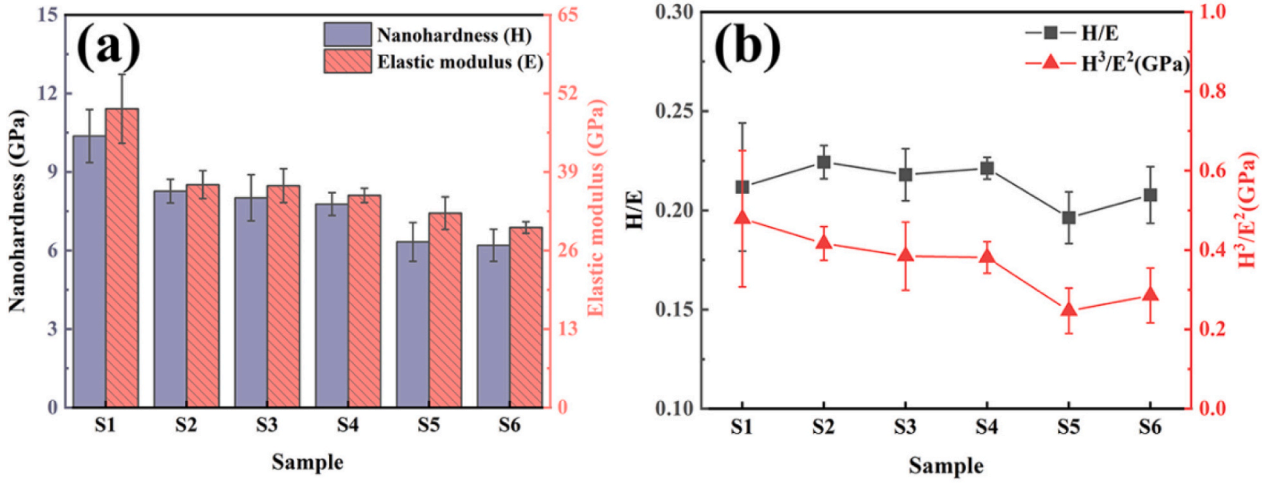

Fig. 4. (a) Hardness (H) and elastic modulus (E), (b) H/E and H^3/E^2 of a-C:H/a-C:H:Si:O coatings.

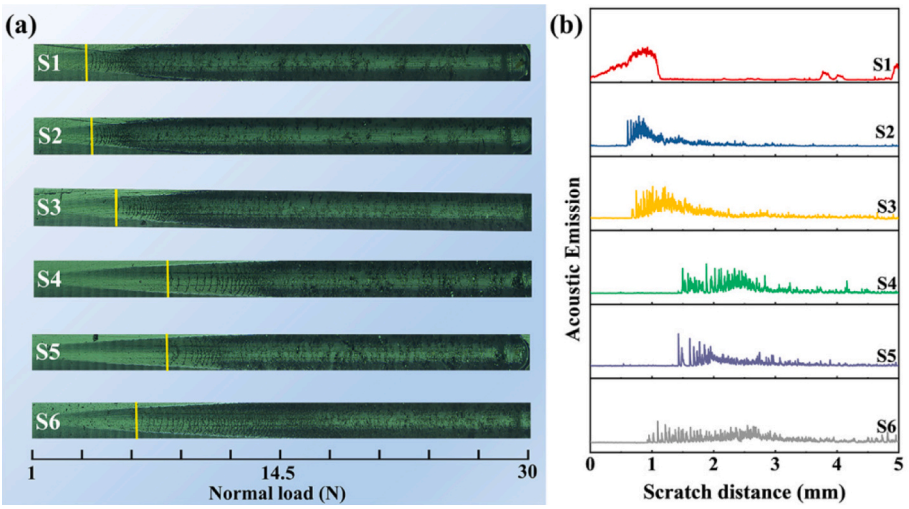

Fig. 5. (a) Scratch morphologies of a-C:H/a-C:H:Si:O coatings and (b) the corresponding acoustic emission signal.

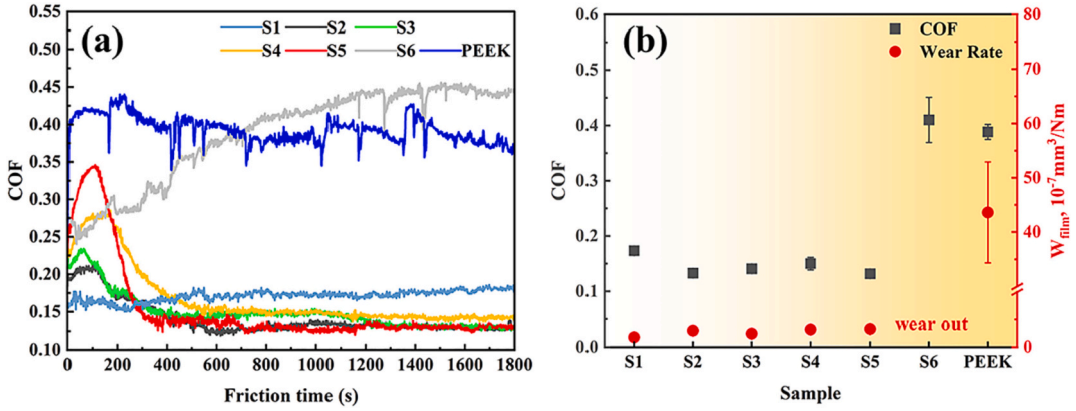

Fig. 6. (a) COF curves and (b) average COF after the running-in stage and wear rate of different samples.

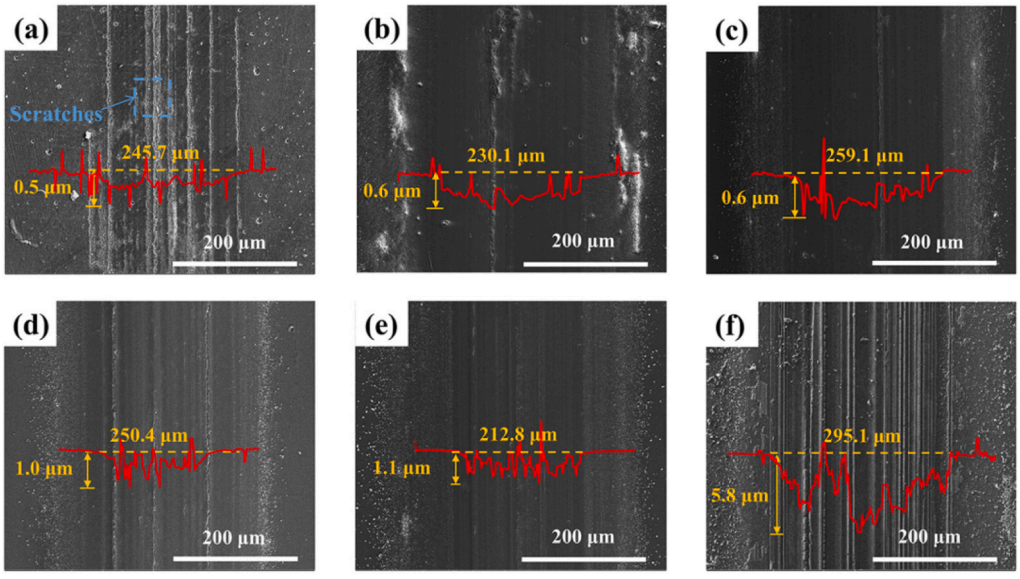

Fig. 7. The surface morphologies after the tribological experiment and the corresponding 2D wear track depth profiles for S1 (a), S2 (b), S3 (c), S4 (d), S5 (e), and S6 (f), respectively.

Fig. S2 provided the schematic illustration of the cross-sectional area of the wear track measurement. For virgin PEEK, it showed an unstable and high COF of around 0.4 during the whole tribological test. For a-C:H coated PEEK (S1), its COF curve was relatively stable at around 0.17, and no running-in period can be observed. For a-C:H:Si:O coated PEEK with HMDSO/C_2H_2 ratio range from 1:10 to 1:4 (S2 ~ S5), each sample exhibited a running-in period from 300 to 500 s, and then followed by a stable and lower COF values of 0.13, 0.14, 0.15 and 0.13, respectively. At HMDSO/C_2H_2 ratio 1/2 (S6), its friction coefficient curve exhibited an exceptionally continuous increasing trend (Fig. 6(a)). After 700 s, its COF was even larger than that of the pristine PEEK. In Fig. 6(b), the wear rate of the virgin PEEK was 4.4×10^{-6} mm^3/Nm, while that of the a-C:H coated sample (S1) was reduced to 1.8×10^{-7} mm^3/Nm. The a-C:H:Si:O coated PEEK (S2 ~ S5) also had a low wear rate of $2.9 \pm 0.4 \times 10^{-7}$ mm^3/Nm, suggesting improved wear resistance. However, sample 6 was worn out.

Fig. 7 presents the representative SEM surface morphologies and the corresponding 2D wear track depth profiles of all coatings after the tribological test. The a-C:H coated sample showed the shallowest wear depth(Fig. 7(a)). Its wear track was 245.7 μm in width and 0.5 μm in depth, which can be attributed to its highest hardness and maximum H^3/E^2 value, namely its best resistance to plastic deformation. However, numerous scratches were found in the wear track of the S1 coating, which may be caused by the poor adhesion strength between a-C:H coating and substrate and its relatively low elastic deformation resistance. The width and depth of the wear tracks of S2, S3, S4, and S5 coatings were 230.1 μm and 0.6 μm, 259.1 μm and 0.6 μm, 250.4 μm and 1.0 μm, 212.8 μm and 1.1 μm (Fig. 7 (b-e)), respectively. And compared with the a-C:H coated sample, all those four wear tracks showed relatively smooth surface morphologies with fewer scratches, which can be explained by the improved adhesion strength and lower H and E values. When the gas flow ratio of HMDSO to C_2H_2 was 1/2 (S6), the wear track was 295.1 μm in width and 5.8 μm in depth (Fig. 7(f)), which exceeded the thickness of the coating. Besides, many particles were scattered on the surface.

Moreover, the surface morphologies and elemental distributions on the mating balls were characterized. In Fig. 8, for a-C:H/a-C:H:Si:O (S1 ~ S6) coated samples, the sizes of the contact area were a diameter of 283.8, 279.3, 265.9, 269.9, 268.4, 408.7 μm, respectively. For a-C:H and a-C:H:Si:O deposited with HMDSO/C_2H_2 ratio range from 1/10 to 1/4 (S1 ~ S5), the contact area on the mating ball was covered with some transfer materials. C, O elements (Fig. 8(a)), or C, Si, and O elements were identified by the corresponding EDS elemental maps (Fig. 8(b-f)), suggesting that the transfer materials were mainly composed of debris from the a-C:H/a-C:H:Si:O coatings. In addition, the transfer materials of the S1 sample mainly accumulated around the wear scar, while for the Si/O co-doped samples (S2 ~ S5), the transfer layer was mainly formed in the center of the wear scar. For the sample 6, though there were some materials transferred from the coating, no dense and intact tribo-film was formed.

The wear rate of the mating ball is an important basis for evaluating the lubricity of the coating. We have summarized the average wear rate of mating ball sliding with different coatings, as shown in Fig. 9. For a-C:H (S1), the wear rate of the mating ball was 11.6×10^{-7} mm^3/Nm. This reflects the excellent lubricity of the amorphous carbon coating. Furthermore, the mating balls sliding with a-C:H:Si:O coatings (S2 ~ S5: Si:3.96– 7.49 at. %, O:3.07– 6.07 at. %) obtained a lower wear rate, and

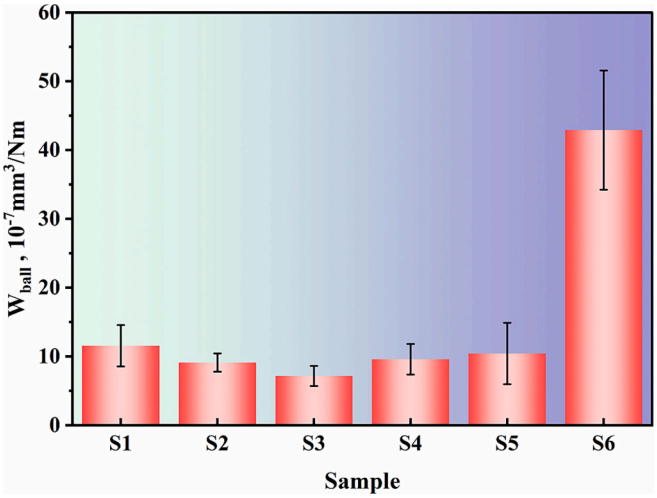

Fig. 9. Wear rates of mating balls.

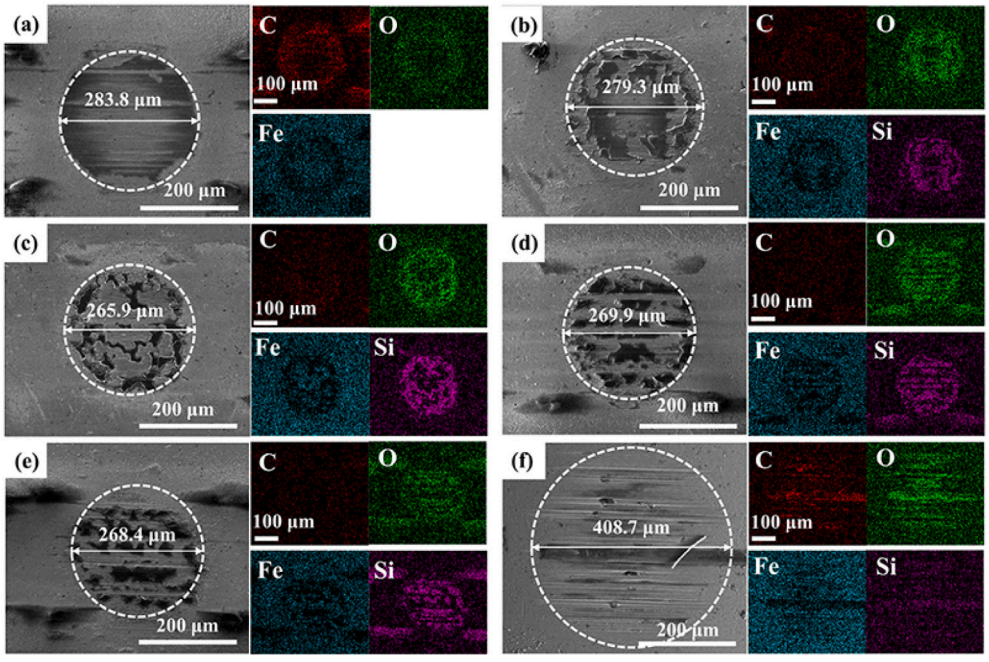

Fig. 8. Surface morphologies and EDS energy spectra of the wear scars on the mating balls for S1 (a), S2 (b), S3 (c), S4 (d), S5 (e), and S6 (f), respectively.

the ball sliding with sample 3 got the lowest wear rate of 7.2×10^{-7} mm^3/Nm, which indicates that co-doping of silicon and oxygen is beneficial to improve the lubricity of the coating. However, for sample 6 (Si:10.0 at. %, O:10.9 at. %, and C:79.1 at. %), the mating ball was seriously worn due to severe damage to the coating, and the wear rate was 42.9×10^{-7} mm^3/Nm.

The transfer materials on the mating balls were investigated with the Raman spectrum. In Fig. 10(a), typical Raman signals of amorphous carbon located at 1000 ~ 2000 cm^{-1} were detected. Combined with EDS analysis (Fig. 8), it indicated that the tribo-film was composed of debris from the deposited coatings. Fig. 10(b) shows the quantitative fitting results. Compared with as-deposited coatings (Fig. 3(b)), the FWHM (G) of the tribo-film did not change evidently. The position of the G peak on S1, S2, and S3 was little changed, but the I_D/I_G value increased from about 0.66 to 1.22. For samples 4 to 6, the position of the G peak increased, and the I_D/I_G also increased slightly, suggesting the graphitization of the tribo-film in different degrees.

4. Discussion

The tribological properties of a-C:H and a-C:H:Si:O coated PEEK should be discussed from the incorporation of silicon and oxygen elements, and the following evolution of mechanical properties and the formation of the tribo-film.

During the tribological test, the contact area between the mating ball and the sample will determine the COF and wear rate of a-C:H or a-C:H:Si:O coated PEEK, Fig. 11 illustrates the schematic diagram of the wear mechanism for various systems. Firstly, due to the significant improvement of the mechanical properties of the sample surface, the PEEK coated by a-C:H or a-C:H:Si:O exhibited a lower wear rate. In addition, the excellent lubricity of amorphous carbon made a major contribution to the reduction of the friction coefficient of coated PEEK. In general, with the application of a-C:H (S1) and a-C:H:Si:O (S2 ~ S5) coatings, the tribological performance of the PEEK were greatly improved.

However, numerous scratches were found in the wear track of the a-C:H coating, which may be related to the poor adhesion strength between a-C:H coating and substrate and its relatively low elastic deformation resistance. This is unfavorable to the long-term stability of the equipment. Compared with pure a-C:H, all a-C:H:Si:O coatings had a lower hardness because the doping of silicon and oxygen will break up the continuity of the amorphous carbon matrix [43,44]. The splinter and delamination of a-C:H:Si:O could appear in the initial stage of the tribological test, due to their degraded mechanical properties, which can explain their longer running-in period. Then, those delaminated materials can be transferred to the mating ball during the sliding process, and the tribo-film can also be formed. In consideration of the higher polar bond fraction of C—Si and C—O, the higher surface energy of the transferred material from the sample 2 to 5 may result in a stronger adhesion force between the tribo-film and the contact area on the mating ball. Furthermore, the C-Si-O on the tribo-film could reduce shear resistance [45]. Therefore, this tribo-film can dominate the following sliding process and result in its stable and lower friction coefficient.

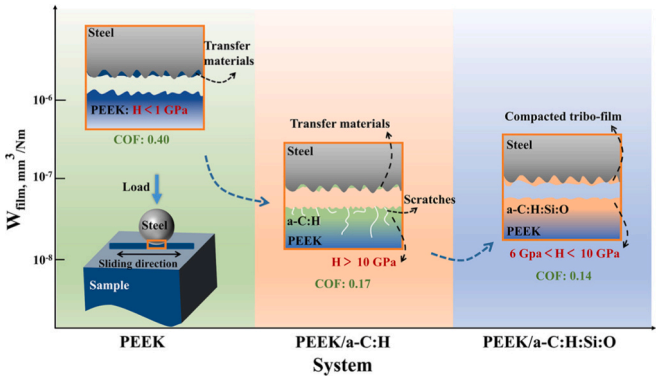

Fig. 11. Schematic diagrams of wear mechanism for various systems.

5. Conclusion

Here, a-C:H and a-C:H:Si:O coatings were prepared on PEEK substrates by the PECVD system using C_2H_2 and HMDSO as precursors. Compared with untreated PEEK with the hardness of 0.2 GPa, the surface hardness of the coated PEEK increased and the wear rate decreased by more than 10 times. With the increase of Si and O concentration, the hardness and plastic deformation resistance (H^3/E^2) of the coating decreased. It was found that the COF of the S2 to S5 was lower than S1, suggesting that the tribo-film played an important role. In summary, considering its mechanical properties and the formation of dense tribo-film, proper Si and O concentration (Si:3.96– 7.49 at. %, O:3.07– 6.07 at. %) in the a-C:H:Si:O coating should be one key factor for improving the tribological performance of PEEK.

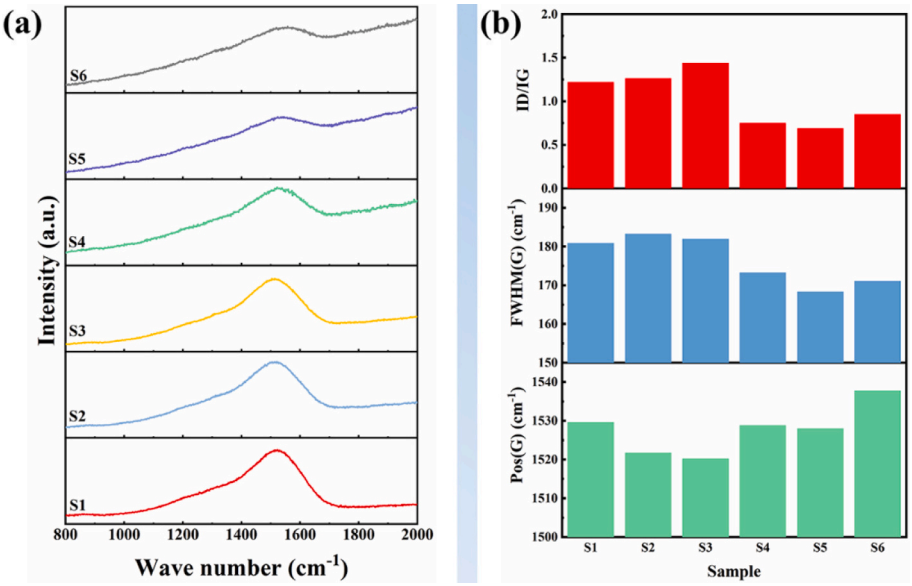

Fig. 10. (a) Raman spectra and (b) fitting results of mating ball worn with a different sample.

CRediT authorship contribution statement

Xianchun Jiang: Formal analysis, Data curation, Writing – original draft. **Peng Guo:** Formal analysis, Writing – review & editing. **Li Cui:** Investigation, Funding acquisition. **Yadong Zhang:** Investigation. **Rende Chen:** Investigation. **Yumin Ye:** Investigation. **Aiying Wang:** Writing – review & editing, Validation, Funding acquisition. **Peiling Ke:** Conceptualization, Supervision, Writing – review & editing, Project administration, Funding acquisition.

Declaration of competing interest

The authors declare that they have no known competing financial interests or personal relationships that could have appeared to influence the work reported in this paper.

Data availability

Data will be made available on request.

Acknowledgments

This work was supported by A-class pilot of the Chinese Academy of Sciences (XDA22010303); CAS Interdisciplinary Innovation Team (292020000008); National Natural Science Foundation of China (52025014); CAS-NST Joint Research Project (174433KYSB20200021); Hubei Province Technology Innovation Major Project (2020BED007); and Zhejiang Natural Science Foundation (LQ20E020004).

Appendix A. Supplementary data

Supplementary data to this article can be found online at https://doi.org/10.1016/j.diamond.2022.109650.

References

[1] H. Wang, M. Xu, W. Zhang, D.T. Kwok, J. Jiang, Z. Wu, P.K. Chu, Mechanical and biological characteristics of diamond-like carbon coated poly aryl-ether-ether-ketone, Biomaterials 31 (2010) 8181–8187, https://doi.org/10.1016/j.biomaterials.2010.07.054.

[2] G. Zhang, W.Y. Li, M. Cherigui, C. Zhang, H. Liao, J.M. Bordes, C. Coddet, Structures and tribological performances of PEEK (poly-ether-ether-ketone)-based coatings designed for tribological application, Prog. Org. Coat. 60 (2007) 39–44, https://doi.org/10.1016/j.porgcoat.2007.06.004.

[3] G. Zhang, C. Zhang, P. Nardin, W.Y. Li, H. Liao, C. Coddet, Effects of sliding velocity and applied load on the tribological mechanism of amorphous poly-ether–ether–ketone (PEEK), Tribol. Int. 41 (2008) 79–86, https://doi.org/10.1016/j.triboint.2007.05.002.

[4] B. Cheng, H. Duan, Q. Chen, H. Shang, Y. Zhang, J. Li, T. Shao, Effect of laser treatment on the tribological performance of polyetheretherketone (PEEK) under seawater lubrication, Appl. Surf. Sci. 566 (2021), 150668, https://doi.org/10.1016/j.apsusc.2021.150668.

[5] H. Liu, J. Wang, P. Jiang, F. Yan, Accelerated degradation of polyetheretherketone and its composites in the deep sea, R. Soc. Open Sci. 5 (2018), 171775, https://doi.org/10.1098/rsos.171775.

[6] B. Wang, S. Yu, J. Mao, Y. Wang, M. Li, X. Li, Effect of basalt fiber on tribological and mechanical properties of polyether-ether-ketone (PEEK) composites, Compos. Struct. 266 (2021), 113847, https://doi.org/10.1016/j.compstruct.2021.113847.

[7] G. Tatsumi, M. Ratoi, Y. Shitara, S. Hasegawa, K. Sakamoto, B.G. Mellor, Mechanism of oil-lubrication of PEEK and its composites with steel counterparts, Wear 486–487 (2021), 204085, https://doi.org/10.1016/j.wear.2021.204085.

[8] Y. Yan, C. Jiang, Y. Huo, C. Li, Preparation and tribological behaviors of lubrication-enhanced PEEK composites, Appl. Sci. 10 (2020) 7536, https://doi.org/10.3390/app10217536.

[9] J. Zhu, L. Ma, R. Dwyer-Joyce, Friction and wear behaviours of self-lubricating peek composites for articulating pin joints, Tribol. Int. 149 (2020), 105741, https://doi.org/10.1016/j.triboint.2019.04.025.

[10] Q.-H. Wang, J. Xu, W. Shen, Q. Xue, The effect of nanometer SiC filler on the tribological behavior of PEEK, Wear 209 (1997) 316–321, https://doi.org/10.1016/S0043-1648(97)00015-X.

[11] M. Wang, The tribological performance of engineered micro-surface topography by picosecond laser on PEEK, Ind. Lubr. Tribol. 72 (2019) 172–179, https://doi.org/10.1108/ilt-06-2019-0202.

[12] F. Zhao, H. Li, L. Ji, Y. Wang, X. Liu, H. Zhou, J. Chen, Effect of microstructural evolution on mechanical and tribological properties of ti-doped DLC films: how was an ultralow friction obtained? J. Vac. Sci. Technol. A 34 (2016) https://doi.org/10.1116/1.4944053.

[13] D. He, C. He, W. Li, L. Shang, L. Wang, G. Zhang, Tribological behaviors of in-situ textured DLC films under dry and lubricated conditions, Appl. Surf. Sci. 525 (2020), 146581, https://doi.org/10.1016/j.apsusc.2020.146581.

[14] H. Cao, J. Momand, A. Syari'ati, F. Wen, P. Rudolf, P. Xiao, J.T.M. De Hosson, Y. Pei, Temperature-adaptive ultralubricity of a WS2/a-C nanocomposite coating: performance from room temperature up to 500 degrees C, ACS Appl. Mater. Interfaces 13 (2021) 28843–28854, https://doi.org/10.1021/acsami.1c06061.

[15] Y.-B. Guo, F. Chau-Nan Hong, Adhesion improvements for diamond-like carbon films on polycarbonate and polymethylmethacrylate substrates by ion plating with inductively coupled plasma, Diam. Relat. Mater. 12 (2003) 946–952, https://doi.org/10.1016/s0925-9635(02)00320-5.

[16] W. Kaczorowski, W. Szymanski, D. Batory, P. Niedzielski, Tribological properties and characterization of diamond like carbon coatings deposited by MW/RF and RF plasma-enhanced CVD method on Poly(ether-ether-ketone), Plasma Process. Polym. 11 (2014) 878–887, https://doi.org/10.1002/ppap.201400025.

[17] Y. Su, Y. Wang, C. Wang, J. Li, W. Guan, W. Guo, Y. Sui, J. Lan, In-situ growing amorphous carbon film with attractive mechanical and tribological adaptability on PEEK via continuous plasma-induced process, Vacuum 187 (2021), 110147, https://doi.org/10.1016/j.vacuum.2021.110147.

[18] R. Matsumoto, K. Sato, K. Ozeki, K. Hirakuri, Y. Fukui, Cytotoxicity and tribological property of DLC films deposited on polymeric materials, Diam. Relat. Mater. 17 (2008) 1680–1684, https://doi.org/10.1016/j.diamond.2008.02.027.

[19] J. Dufils, F. Faverjon, C. Héau, C. Donnet, S. Benayoun, S. Valette, Evaluation of a variety of a-C: H coatings on PEEK for biomedical implants, Surf. Coat. Technol. 313 (2017) 96–106, https://doi.org/10.1016/j.surfcoat.2017.01.032.

[20] J. Peng, Y. Xiao, M. Yang, J. Liao, Effect of nitrogen doping on the microstructure and thermal stability of diamond-like carbon coatings containing silicon and oxygen, Surf. Coat. Technol. 421 (2021), 127479, https://doi.org/10.1016/j.surfcoat.2021.127479.

[21] T. Xu, L. Pruitt, Diamond-like carbon coatings for orthopaedic applications: an evaluation of tribological performance, J. Mater. Sci. Mater. Med. 10 (1999) 83–90, https://doi.org/10.1023/A:1008916903171.

[22] N. Moolsradoo, S. Abe, S. Watanabe, Thermal stability and tribological performance of DLC-Si–O films, Adv. Mater. Sci. Eng. 2011 (2011) 1–7, https://doi.org/10.1155/2011/483437.

[23] L.K. Randeniya, A. Bendavid, P.J. Martin, M.S. Amin, E.W. Preston, F.S. Magdon Ismail, S. Coe, Incorporation of si and SiO(x) into diamond-like carbon films: impact on surface properties and osteoblast adhesion, Acta Biomater. 5 (2009) 1791–1797, https://doi.org/10.1016/j.actbio.2009.01.013.

[24] S.-M. Baek, T. Shirafuji, N. Saito, O. Takai, Adhesion property of SiOx-doped diamond-like carbon films deposited on polycarbonate by inductively coupled plasma chemical vapor deposition, Thin Solid Films 519 (2011) 6678–6682, https://doi.org/10.1016/j.tsf.2011.04.080.

[25] D. Zhang, S. Li, X. Zuo, P. Guo, P. Ke, A. Wang, Structural and mechanism study on enhanced thermal stability of hydrogenated diamond-like carbon films doped with Si/O, Diam. Relat. Mater. 108 (2020), 107923, https://doi.org/10.1016/j.diamond.2020.107923.

[26] I. Masami, M. Haruho, M. Tatsuya, C. Junho, Low temperature si-DLC coatings on fluoro rubber by a bipolar pulse type PBII system, Surf. Coat. Technol. 206 (2011) 999–1002, https://doi.org/10.1016/j.surfcoat.2011.04.011.

[27] N. Graupner, K. Albrecht, D. Hegemann, J. Müssig, Plasma modification of man-made cellulose fibers (Lyocell) for improved fiber/matrix adhesion in poly(lactic acid) composites, J. Appl. Polym. Sci. 128 (2013) 4378–4386, https://doi.org/10.1002/app.38663.

[28] W.C. Oliver, G.M. Pharr, An improved technique for determining hardness and elastic modulus using load and displacement sensing indentation experiments, J. Mater. Res. 7 (2011) 1564–1583, https://doi.org/10.1557/jmr.1992.1564.

[29] H. Sun, F. Lei, T. Li, H. Han, B. Li, D. Li, D. Sun, Facile fabrication of novel multifunctional lubricant-infused surfaces with exceptional tribological and anticorrosive properties, ACS Appl. Mater. Interfaces 13 (2021) 6678–6687, https://doi.org/10.1021/acsami.0c21667.

[30] J. Wei, P. Guo, H. Li, P. Ke, A. Wang, Insights on high temperature friction mechanism of multilayer ta-C films, J. Mater. Sci. Technol. 97 (2022) 29–37, https://doi.org/10.1016/j.jmst.2021.04.028.

[31] F. Mangolini, J. Hilbert, J.B. McClimon, J.R. Lukes, R.W. Carpick, Thermally induced structural evolution of silicon- and oxygen-containing hydrogenated amorphous carbon: a combined spectroscopic and molecular dynamics simulation investigation, Langmuir 34 (2018) 2989–2995, https://doi.org/10.1021/acs.langmuir.7b04266.

[32] M.R. Alexander, R.D. Short, F.R. Jones, W. Michaeli, C.J. Blomfield, A study ofHMDSO/O2 plasma deposits using a high-sensitivity and -energy resolution XPS instrument: curve fitting of the si 2p core level, Appl. Surf. Sci. 137 (1999) 179–183, https://doi.org/10.1016/S0169-4332(98)00479-6.

[33] Š. MeŠKinis, A. TamuleviČIenĖ, Structure, properties and applications of diamond like nanocomposite (SiOx containing DLC) films: a review, Mater. Sci. 17 (2011) 358–370, https://doi.org/10.5755/j01.ms.17.4.770.

[34] Z.C. Li, Y.X. Wang, X.Y. Cheng, Z.X. Zeng, J.L. Li, X. Lu, L.P. Wang, Q.J. Xue, Continuously growing ultrathick CrN coating to achieve high load-bearing capacity and good tribological property, ACS Appl. Mater. Interfaces 10 (2018) 2965–2975, https://doi.org/10.1021/acsami.7b16426.

[35] C.Q. Dang, J.L. Li, Y. Wang, J.M. Chen, Structure, mechanical and tribological properties of self -toughening TiSiN/Ag multilayer coatings on Ti6A14V prepared by arc ion plating, Appl. Surf. Sci. 386 (2016) 224–233, https://doi.org/10.1016/j.apsusc.2016.06.024.

[36] J. Shuai, X. Zuo, Z. Wang, L. Sun, R. Chen, L. Wang, A. Wang, P. Ke, Erosion behavior and failure mechanism of Ti/TiAlN multilayer coatings eroded by silica sand and glass beads, J. Mater. Sci. Technol. 80 (2021) 179–190, https://doi.org/10.1016/j.jmst.2021.01.001.
[37] Y. Wang, W. Guan, C.B. Fischer, S. Wehner, R. Dang, J. Li, C. Wang, W. Guo, Microstructures, mechanical properties and tribological behaviors of amorphous carbon coatings in-situ grown on polycarbonate surfaces, Appl. Surf. Sci. 563 (2021), 150309, https://doi.org/10.1016/j.apsusc.2021.150309.
[38] X. Cao, W.F. He, G.Y. He, B. Liao, H.H. Zhang, J. Chen, C.L. Lv, Sand erosion resistance improvement and damage mechanism of TiAlN coating via the bias-graded voltage in FCVA deposition, Surf. Coat. Technol. 378 (2019), 125009, https://doi.org/10.1016/j.surfcoat.2019.125009.
[39] K. Shu, C. Zhang, D. Sun, B. Wu, Z. Li, J. Wu, D. Zheng, L. Gu, Contact cracking and delamination of thin solid lubricating films on deformable substrates, Tribol. Int. 163 (2021), 107181, https://doi.org/10.1016/j.triboint.2021.107181.
[40] Y. Yang, H. Shang, T. Shao, Influence of nitrogen implantation on adhesion strength of TiAlN film on γ-TiAl alloy, Appl. Surf. Sci. 508 (2020), 145141, https://doi.org/10.1016/j.apsusc.2019.145141.
[41] S. Zhang, F. Awaja, N. James, D.R. McKenzie, A.J. Ruys, Autohesion of plasma treated semi-crystalline PEEK: comparative study of argon, nitrogen and oxygen treatments, Colloids Surf. A Physicochem. Eng. Asp. 374 (2011) 88–95, https://doi.org/10.1016/j.colsurfa.2010.11.013.
[42] W. Kaczorowski, D. Batory, W. Szymanski, P. Niedzielski, Evaluation of the surface properties of PEEK substrate after two-step plasma modification: etching and deposition of DLC coatings, Surf. Coat. Technol. 265 (2015) 92–98, https://doi.org/10.1016/j.surfcoat.2015.01.053.
[43] D. Neerinck, P. Persoone, M. Sercu, A. Goel, D. Kester, D. Bray, Diamond-like nanocomposite coatings (a-C:H/a-si:O) for tribological applications, Diam. Relat. Mater. 7 (1998) 468–471, https://doi.org/10.1016/S0925-9635(97)00201-X.
[44] W.J. Yang, Y.-H. Choa, T. Sekino, K.B. Shim, K. Niihara, K.H. Auh, Thermal stability evaluation of diamond-like nanocomposite coatings, Thin Solid Films 434 (2003) 49–54, https://doi.org/10.1016/s0040-6090(03)00466-8.
[45] B. Huang, L.-T. Liu, S. Han, H.-M. Du, Q. Zhou, E.-G. Zhang, Effect of deposition temperature on the microstructure and tribological properties of si-DLC coatings prepared by PECVD, Diam. Relat. Mater. 129 (2022), https://doi.org/10.1016/j.diamond.2022.109345.